ISSN No:-2456-2165 https://doi.org/10.38124/ijisrt/26jun1365

# Comparative Analysis of Independent Steering Strategies for Mobile Robots

Kien Thi Ha My[1]; Pham Quoc Phong[1*]; Le Quoc Chuan[1]

[1]College of Engineering and Technology, Tra Vinh University, Vietnam

Corresponding Author: Pham Quoc Phong[1*]

Publication Date: 2026/07/04

**Abstract: Steering control methods for mobile robots are investigated in this study to optimize maneuverability and terrain adaptability within complex industrial and agricultural environments. Three independent steering configurations—two-front-wheel steering, four-wheel opposite-direction steering, and four-wheel same-direction steering—are mathematically modeled and simulated in the MATLAB/Simulink environment. To empirically validate the theoretical models, a physical four-wheel independent steering prototype was constructed and evaluated. Through a comparative analysis based on turning radius, maneuverability, and trajectory stability, it is demonstrated that the turning radius for confined spaces is significantly minimized by the opposite-direction steering configuration, whereas rapid diagonal transitions are facilitated by the same-direction configuration. Furthermore, the experimental trajectories are shown to align closely with the simulations, yielding a relative error of less than 4%, thereby confirming the reliability of the proposed control strategies. Ultimately, a comprehensive quantitative and qualitative framework is provided to assist in the selection of optimal steering mechanisms for mobile robots.**

***Keywords:*** *Mobile Robot, Four-Wheel Independent Steering, Kinematic Modeling, Experimental Validation, MATLAB/Simulink.*

**How to Cite:** Kien Thi Ha My; Pham Quoc Phong; Le Quoc Chuan (2026) Comparative Analysis of Independent Steering Strategies for Mobile Robots. *International Journal of Innovative Science and Research Technology*, 11(6), 2384-2396. https://doi.org/10.38124/ijisrt/26jun1365

## I. INTRODUCTION

In the field of mobile robotics, precise and flexible navigation plays a pivotal role in ensuring operational performance, terrain adaptability, and system stability in complex environments. Particularly, the selection of an appropriate steering strategy directly influences maneuverability, turning radius, and responsiveness when executing autonomous tasks such as obstacle avoidance, trajectory tracking, or navigating narrow spaces [1, 2].

Various steering configurations have been studied and applied to mobile robots, the most common of which include: Front-Wheel Steering (FWS) [3], Four-Wheel Steering in opposite directions (4WS, opposite-phase or crabless mode) [4, 5], and Four-Wheel Steering in the same direction (4WS, in-phase or crab mode). Each configuration has distinct advantages and disadvantages regarding turning capability, motion stability, and control complexity [6]. Previous studies have shown that the 4WS system offers a smaller turning radius and significantly improves stability during high-speed lane changes, whereas the FWS is simpler and more popular in low-cost applications [7]. Notably, when considering independent steering control for each axle, the difference between opposite-direction 4WS and same-direction 4WS creates entirely different kinematic characteristics, strongly affecting the robot's trajectory and adaptability [8].

While numerous studies have extensively discussed the theoretical pros and cons of each steering system, comprehensive research integrating mathematical modeling with rigorous experimental verification on physical hardware remains relatively limited. Therefore, this research develops a mathematical simulation model on the MATLAB/Simulink platform to evaluate the kinematic distribution and response capabilities of the system under different steering modes. The simulation model analyzes the impact of control parameters such as steering angle and steering methods in various operational scenarios. Concurrently, a physical prototype is constructed to empirically verify the simulation, ensuring objective evaluations. The research results provide a robust theoretical and practical foundation for selecting and designing optimal intelligent controllers for new-generation autonomous robot systems in industrial and agricultural environments.

## II. RELATED WORKS AND METHODOLOGY

- *Related Works*

Numerous studies have proposed various steering mechanisms and control methods to enhance maneuverability, reduce turning radius, facilitate ease of control, and enable

ISSN No:-2456-2165 https://doi.org/10.38124/ijisrt/26jun1365

largescale deployment. The proposed steering configurations include differential drive robots, Ackermann steering robots, and omnidirectional robots, coupled with control algorithms such as adaptive PI and adaptive PID using fuzzy neural networks [9–11].

Despite significant achievements, current research still primarily focuses on developing control algorithms for differential drive configurations or evaluating results through simulation models. Studies on the specific impact of individual steering control methods on the kinematic characteristics of robots, as well as the selection of optimal steering mechanisms for applications in logistics and smart agriculture, remain limited.

Based on these requirements, a mathematical simulation model was constructed in the MATLAB/Simulink environment in this study to investigate steering control methods. The control algorithms implemented in the simulation are verified on a physical model using standard microcontroller boards. Through different steering control methods, the steering angles of each wheel are recorded, evaluated, and compared to assess the accuracy and stability of the model.

The research results not only clarify the influence of steering control methods on the mobility of mobile robots but also provide an important scientific basis for selecting and developing appropriate control systems for autonomous robots applied in logistics, smart agriculture, and work environments demanding high maneuverability and precision.

➢ *Mechanical Structure*

To evaluate and validate the proposed steering control methods, a physical four-wheel independent steering (4WIS) mobile robot prototype was designed and constructed. Fig. 1 illustrates the overall 3D mechanical configuration of the developed system. The robot frame features a compact layout with a base length (L) of 0.66 m, a base width (W) of 0.482 m, and a wheel radius of 0.125 m.

The propulsion system utilizes high-torque Brushless DC (BLDC) motors to ensure stable speed response across diverse terrains. For the independent steering mechanism at each wheel module, a high-torque NEMA 86 stepper motor is paired with a Worm Gear Reducer featuring a 1:15 reduction ratio. The selection of the worm gear mechanism is critical; its inherent self-locking capability effectively prevents external ground reaction forces and terrain disturbances from back-driving the steering system. This configuration significantly reduces the holding torque required by the stepper motors, thereby ensuring precise and stable steering angle maintenance during operation. The entire mechanical system is rigidly supported by custom-designed fixed brackets and powered by a centralized onboard Accu battery network.

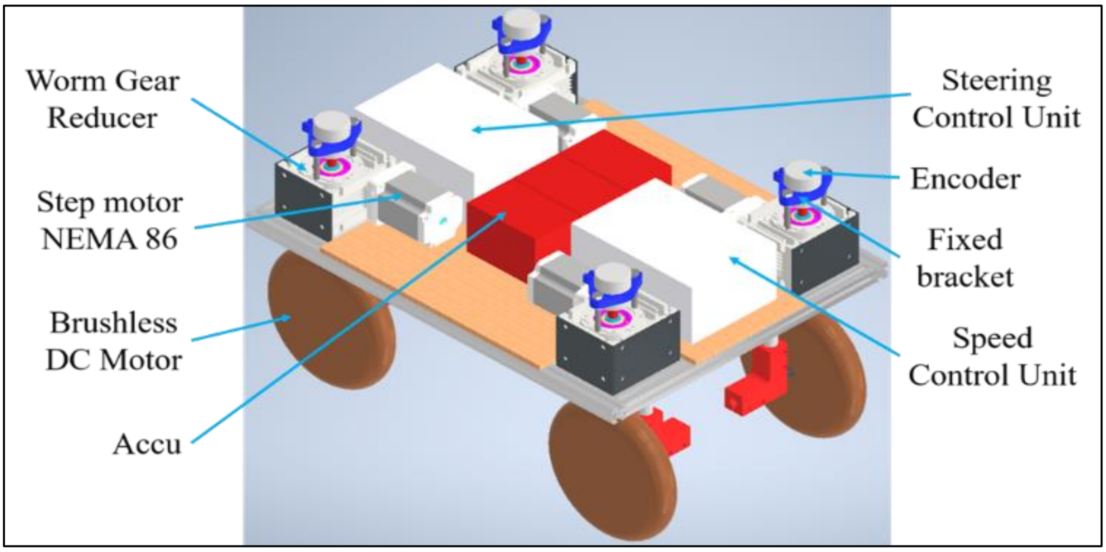


Fig 1 Overall 3D Model of the Developed Mobile Robot

➢ *Control Architecture*

The electronic wiring layout and the distributed control architecture of the mobile robot are comprehensively depicted in Fig. 2. The central processing unit (CPU) is built upon an Arduino UNO microcontroller, programmed in a native C/C++ environment to handle real-time kinematic distribution equations and multi-sensor data fusion.

To achieve autonomous 4WIS steering control, each wheel's angular position is independent and managed by a dedicated TB6600 stepper motor driver. The primary power distribution relies on a 36V DC battery bank. A step-down Buck Converter is employed to regulate the voltage from 36V to 12V DC, supplying safe operating power to the microcontroller, auxiliary relays, and measurement circuits.

For high-precision closed-loop angular feedback, each steering axle is coupled with a two-phase quadrature optical encoder offering a resolution of 600 pulses per revolution (PPR). The incremental feedback signals are continuously transmitted back to the microcontroller's hardware interrupt pins for real-time analysis, angular error processing, and immediate control adjustment, ensuring highly accurate steering response.

ISSN No:-2456-2165 https://doi.org/10.38124/ijisrt/26jun1365

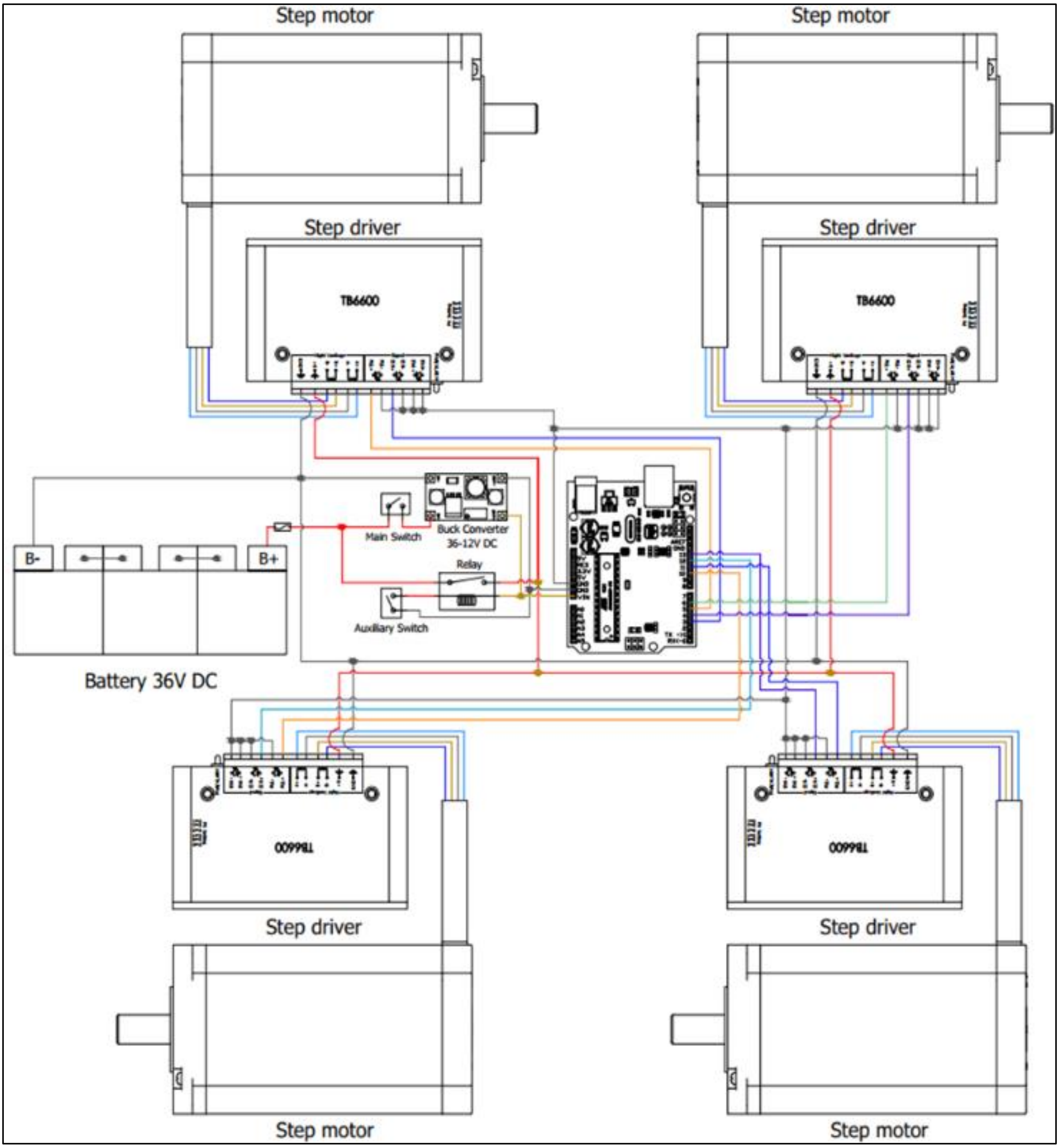


Fig 2 Electrical Wiring and Component Layout of the Robot Control System

- *System Algorithm Development*

To investigate the impact of each control strategy on the steering angle, this paper uses a four-wheel independent steering configuration that allows each wheel to be steered entirely independently, optimizing the vehicle's maneuverability and kinematic stability [12, 13].

Control method No. 1 (Fig. 3) uses a two-front-wheel steering configuration, similar to the traditional Ackermann steering mechanism commonly used in automobiles and mobile robots. In this configuration, only the two front wheels participate in directional control, while the two rear wheels serve as driving wheels to maintain trajectory stability.

ISSN No:-2456-2165 https://doi.org/10.38124/ijisrt/26jun1365

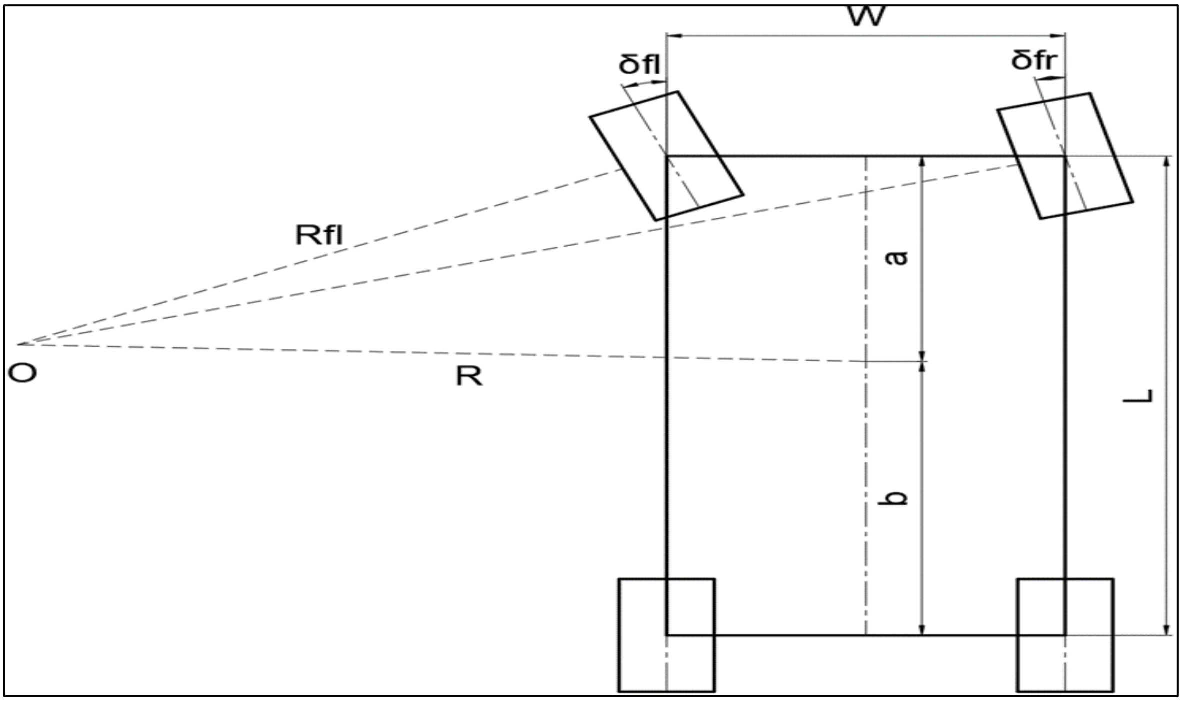

Fig 3 Two-Front-Wheel Steering Control Method

Control method No. 2 (Fig. 4) applies a four-wheel opposite-direction steering mechanism, where the two rear wheels turn in the opposite direction to the two front wheels. This method significantly reduces the turning radius, enhances maneuverability, and limits wheel slip when turning in narrow spaces.

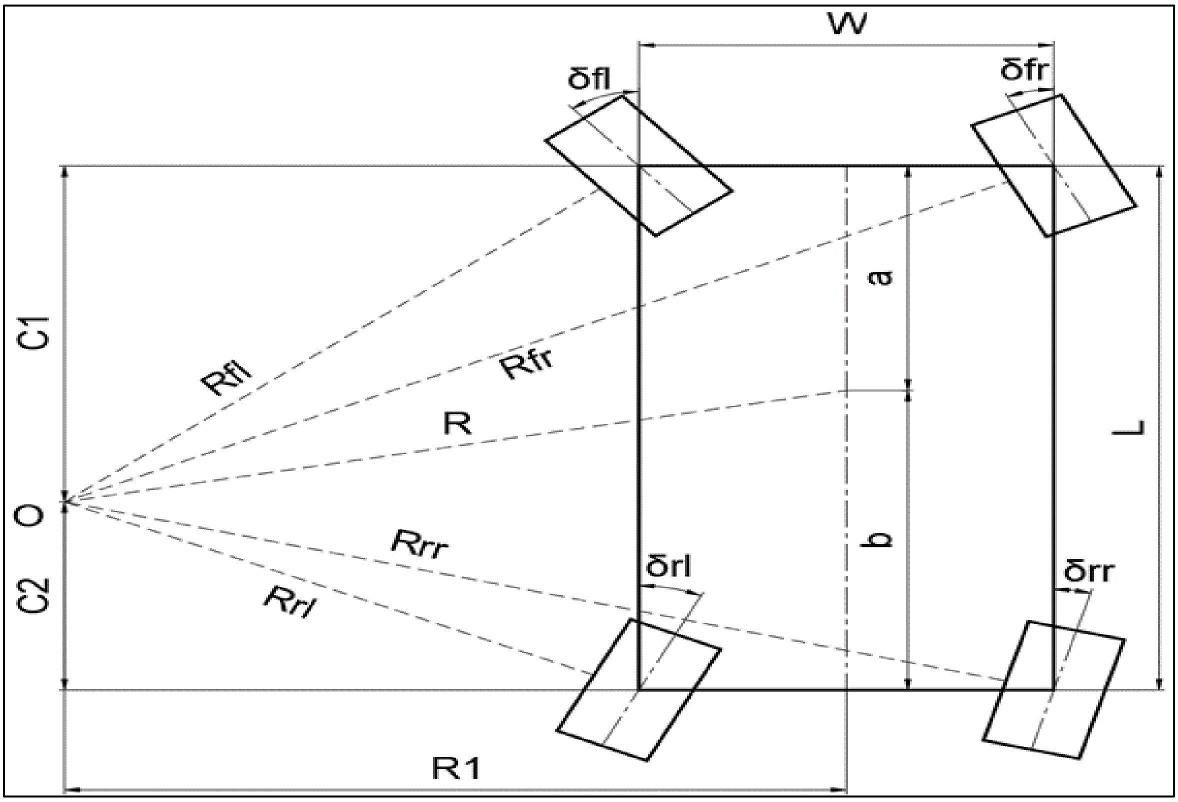

Fig 4 Four-Wheel Independent Steering Control Method, Opposite Direction

Control method No. 3 (Fig. 5) uses a four-wheel same-direction steering mechanism, where all four wheels are controlled to turn in the same direction. This configuration allows the robot to rapidly change direction, perform diagonal trajectories, and improve obstacle avoidance capabilities, making it ideal for high-speed operation.

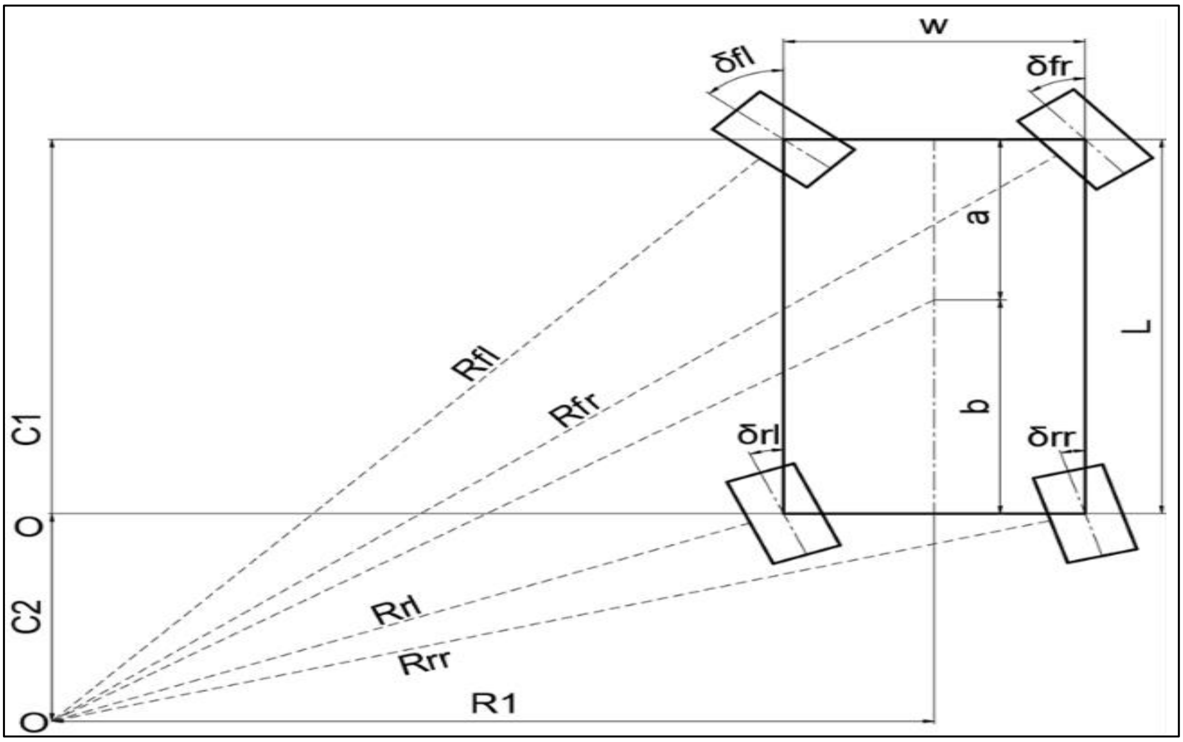


Fig 5 Four-Wheel Independent Steering Control Method, Same Direction

In control method No. 1, the steering angle is determined according to Ackermann steering geometry equations to ensure all wheels move around a common instantaneous center of rotation [14]. The relationship is expressed in Equation (1).

$$\delta_i = \tan^{-1}\left(\frac{L}{R-\frac{W}{2}}\right),\ \delta_o = \tan^{-1}\left(\frac{L}{R+\frac{W}{2}}\right) \quad (1)$$

For control method No. 2, the four-wheel opposite-direction steering equations are applied [15]. At low speeds:

$$\delta_{fl} = \tan^{-1}\left(\frac{C_1}{R_1 - \frac{W}{2}}\right), \qquad \delta_{fr} = \tan^{-1}\left(\frac{C_1}{R_1 + \frac{W}{2}}\right)$$

$$\delta_{rl} = -\tan^{-1}\left(\frac{C_2}{R_1-\frac{W}{2}}\right),\ \delta_{rr} = -tan^{-1}\left(\frac{C_2}{R_1+\frac{W}{2}}\right) \quad (2)$$

Similarly, for control method No. 3, the four-wheel same-direction steering equations are applied [15].

$$\delta_{fl} = \tan^{-1}\left(\frac{C_1}{R_1 - \frac{W}{2}}\right), \qquad \delta_{fr} = \tan^{-1}\left(\frac{C_1}{R_1 + \frac{W}{2}}\right)$$

$$\delta_{rl} = \tan^{-1}\left(\frac{C_2}{R_1-\frac{W}{2}}\right),\ \delta_{rr} = tan^{-1}\left(\frac{C_2}{R_1+\frac{W}{2}}\right) \quad (3)$$

Equations (1) to (3) contain geometric variables directly related to Fig. 3, 4, and 5, where: $L$ and $W$ are the wheelbase and track width of the model; $R$ is the turning radius; $\delta_i$ and $\delta_o$ are inner and outer steering angles; $C_1$ and $C_2$ are longitudinal distances to the projection axis of the instantaneous rotation center; $R_1$ is the transverse distance from the rotation center to the geometric center.

➢ *Modeling on MATLAB/Simulink*

To preliminary evaluate the kinematic distribution and transient response of the system before physical deployment, a numerical simulation model of the four-wheel independent steering (4WIS) architecture was developed within the MATLAB/Simulink environment. As shown in Fig. 6, the simulation layout is deliberately designed to mirror the actual hardware control loop by integrating several core computational components. Specifically, the Signal Builder block generates the dynamic global steering trajectories over time to represent user navigation commands. This signal is then fed into the MATLAB Function block, which embeds the inverse kinematic equations. By receiving the global steering command alongside the physical dimensions of the prototype ($L$ = 0.66 m, $W$ = 0.482 m), this block calculates the precise reference turning angles for each decoupled wheel ($\delta_{fl}$,$\delta_{fr}$,$\delta_{rl}$,$\delta_{rr}$). Subsequently, a PID Controller block is implemented to replicate the closed-loop error-correction logic programmed into the actual Arduino UNO microcontroller. Furthermore, to accurately reflect real-world mechatronic constraints, Transfer Fnc blocks are integrated to mathematically approximate the mechanical inertia, actuation delays, and transient response of the Nema 86 stepper motors coupled with the 1:15 worm gear reducers. Ultimately, this comprehensive modeling approach allows for the rigorous tuning of control parameters and the verification of geometric synchronization across different steering modes without the risk of mechanical damage to the physical prototype.

ISSN No:-2456-2165 https://doi.org/10.38124/ijisrt/26jun1365

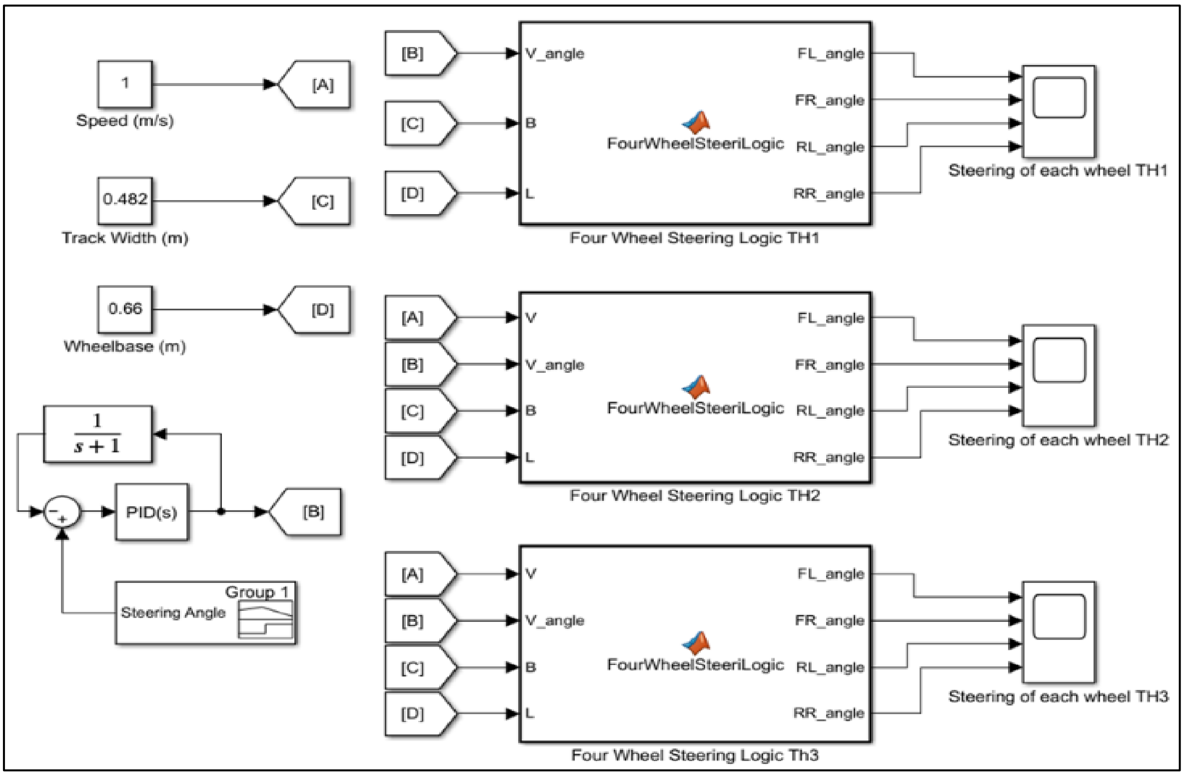

Fig 6 Kinematic Simulation Model and Control Loop Constructed in MATLAB/Simulink

➢ *Experimental Setup*

To empirically validate the numerical simulations and assess the feasibility of practical deployment, a physical four-wheel independent steering (4WIS) mobile robot prototype was constructed and evaluated. The experimental testbench, illustrated in Fig. 7, was arranged to replicate the operational conditions defined in the theoretical models. The primary hardware specifications and dimensional parameters of the prototype are summarized in Table 1.

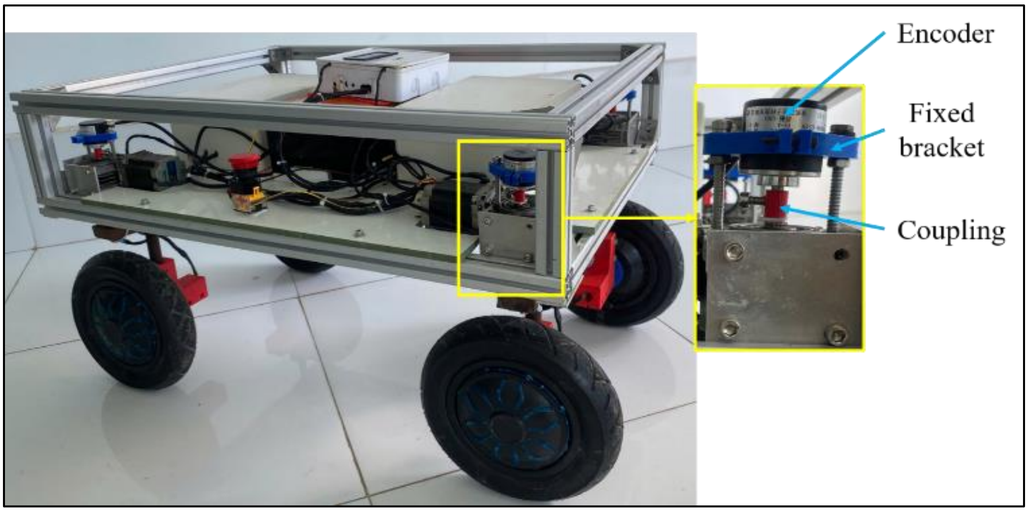

Fig 7 Experimental Setup and Physical Hardware Arrangement of the Mobile Robot

Table 1 Technical Specifications of the Experimental Prototype

| **Hardware Component** | **Specifications** |
|---|---|
| Central processing board | Arduino Uno |
| Steering motors | 4 Nema 86 stepper motors |
| Transmission | 4 Worm gear reducers (1:15) |
| Sensors | 4 Two-phase optical encoders (600 pulses/rev) |
| Power source | 3 DC lead-acid batteries (36V) |
| Model dimensions | L = 0.66 m; W = 0.482 m |
| Wheel radius | 0.125 m |

ISSN No:-2456-2165 https://doi.org/10.38124/ijisrt/26jun1365

The directional actuation of the platform is facilitated by four independent Nema 86 stepper motors. Each motor is coupled with a worm gear reducer to lower the dynamic load during cornering maneuvers. This specific mechanical pairing was selected due to the inherent self-locking characteristic of the worm gears, which acts as a mechanical brake. Consequently, the steering actuators are isolated from external terrain impacts, and unintended back-driving is prevented, thereby maintaining trajectory stability.

For closed-loop performance monitoring and data acquisition, two-phase optical encoders with a resolution of 600 pulses per revolution (PPR) are coaxially mounted to each steering pivot. During the experimental trials, predefined steering profiles were executed by the Arduino UNO controller. The real-time angular displacement of each wheel is continuously captured by the encoders, and this empirical data is fed back to the measurement circuit for analysis. This procedure allows for a direct and objective comparative assessment against the idealized Simulink trajectories.

## III. RESULTS AND DISCUSSION

➢ *Analysis of Simulation Results*

Simulation experiments were conducted over 20 seconds to evaluate the steering characteristics of the robot under three different control methods. The steering input signal is shown in Fig. 8. From 0 to 2 seconds, the robot moves straight. From 2 to 3 seconds, the steering angle changes linearly from $0^0$ to $-5^0$, and then values are maintained in steps for 5 seconds each. The negative steering angle corresponds to the robot turning right.

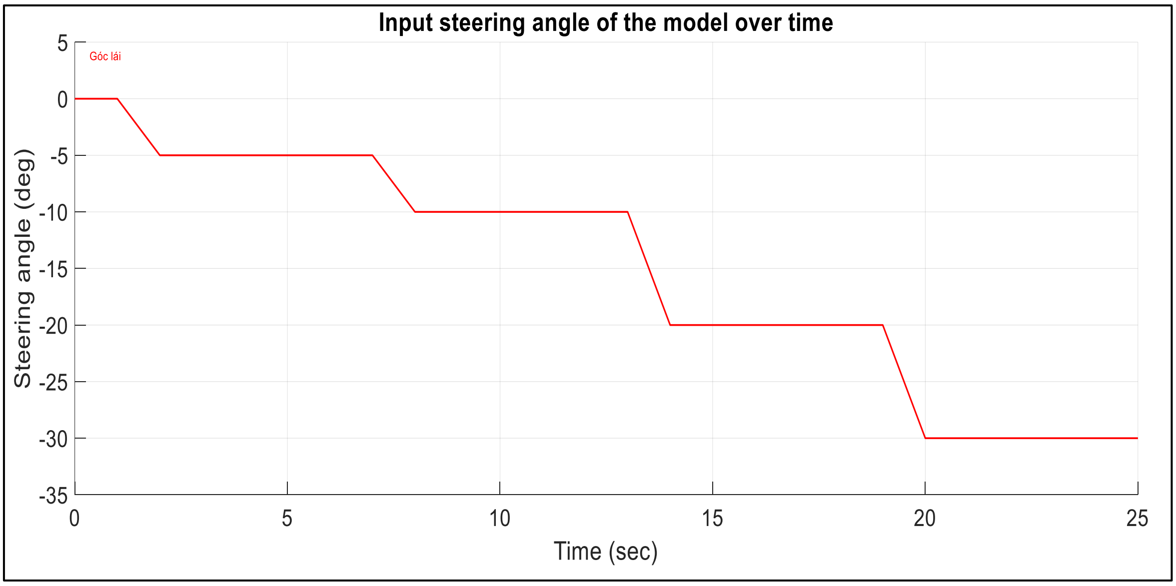


Fig 8 Input Steering Angle of the Model Over Time

The simulation results in Fig. 9 show that in method 1, only the two front wheels participate in steering. At small angles ($-5^0$ and $-10^0$), the difference between the front wheels is around $1.5^0$. At $-30^0$, the difference increases to about $10^0$. While simple, this method may cause lateral slip at large angles, leading to energy loss and tire wear (Table 2, Fig. 10).


Fig 9 Simulated Steering Angles of Each Wheel in Method 1

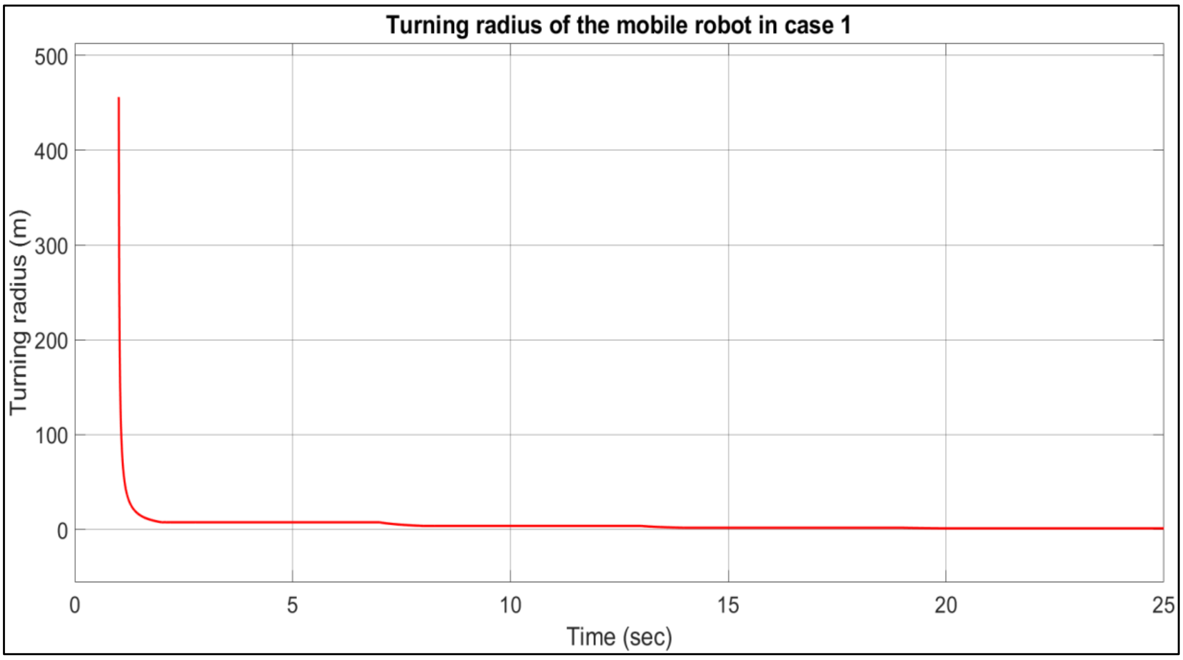


Fig 10 Turning Radius in Method 1

Table 2 Detailed Turning Radius for Method 1

| Steering Angle ($^0$) | Turning Radius (m) |
|---|---|
| -5 | 7,54 |
| -10 | 3,74 |
| -20 | 1,81 |
| -30 | 1,14 |

In method 2 (Fig. 11), all wheels are steered synchronously with the front and rear axles in opposite directions, reducing the turning radius and wheel slip (Table 3, Fig. 12).

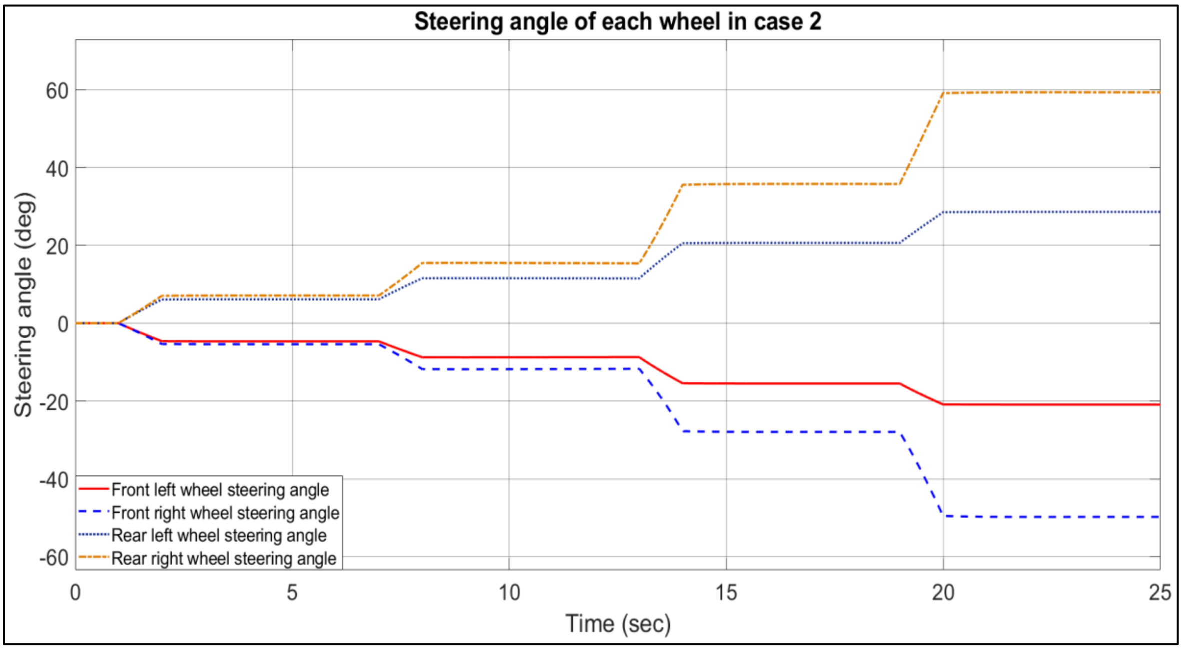


Fig 11 Simulated Steering Angles of Each Wheel in Method 2

ISSN No:-2456-2165 https://doi.org/10.38124/ijisrt/26jun1365

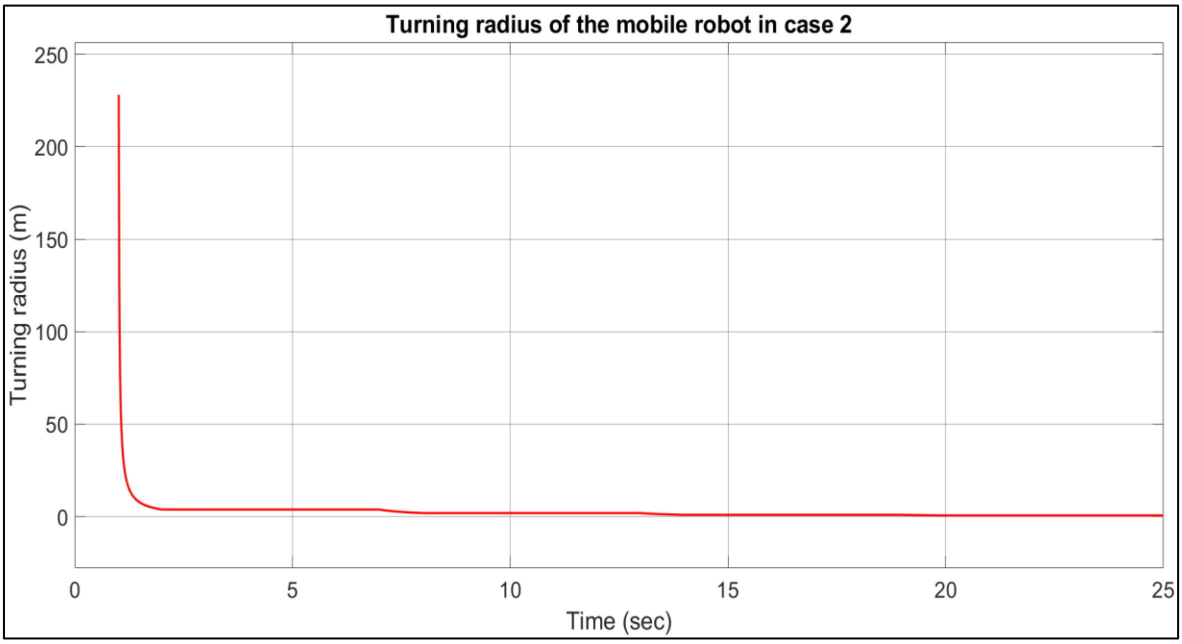

Fig 12 Turning Radius in Method 2

Table 3 Detailed Turning Radius for Method 2

| **Steering Angle ($^0$)** | **Turning Radius (m)** |
|---|---|
| -5 | 3,77 |
| -10 | 1,87 |
| -20 | 0,90 |
| -30 | 0,57 |

In method 3 (Fig. 13), wheels are steered in the same direction, allowing diagonal translation suitable for rapid obstacle avoidance (Table 4, Fig. 14). However, it does not reduce the turning radius as effectively as method 2.

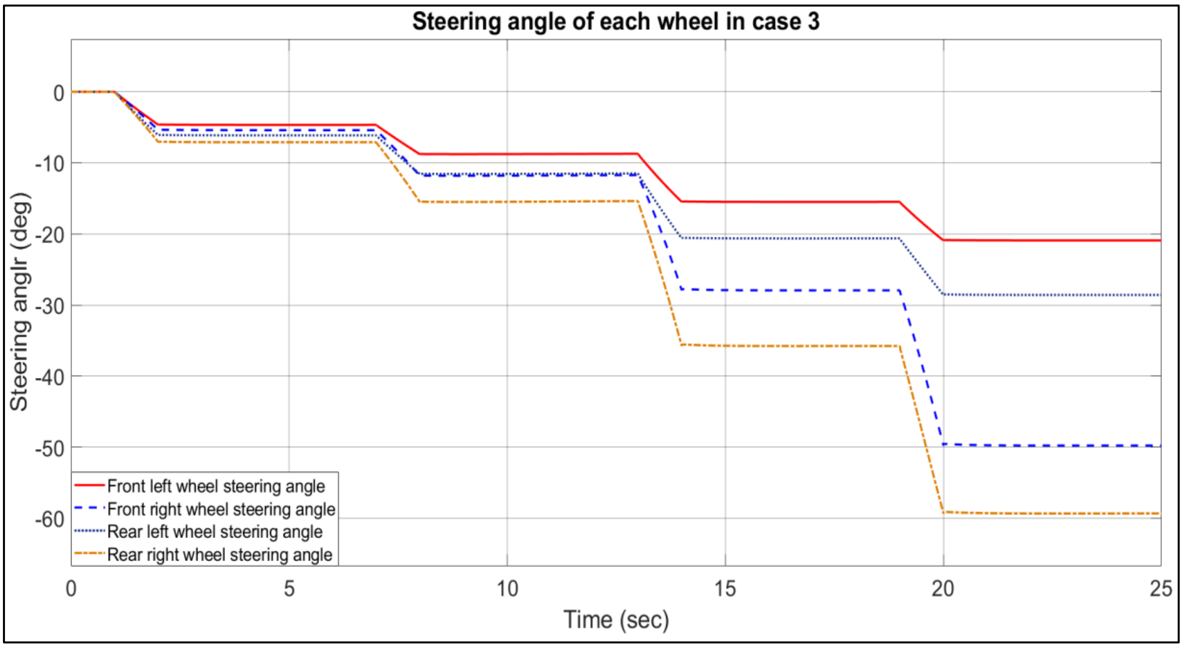

Fig 13 Simulated Steering Angles of Each Wheel in Method 3

ISSN No:-2456-2165 https://doi.org/10.38124/ijisrt/26jun1365

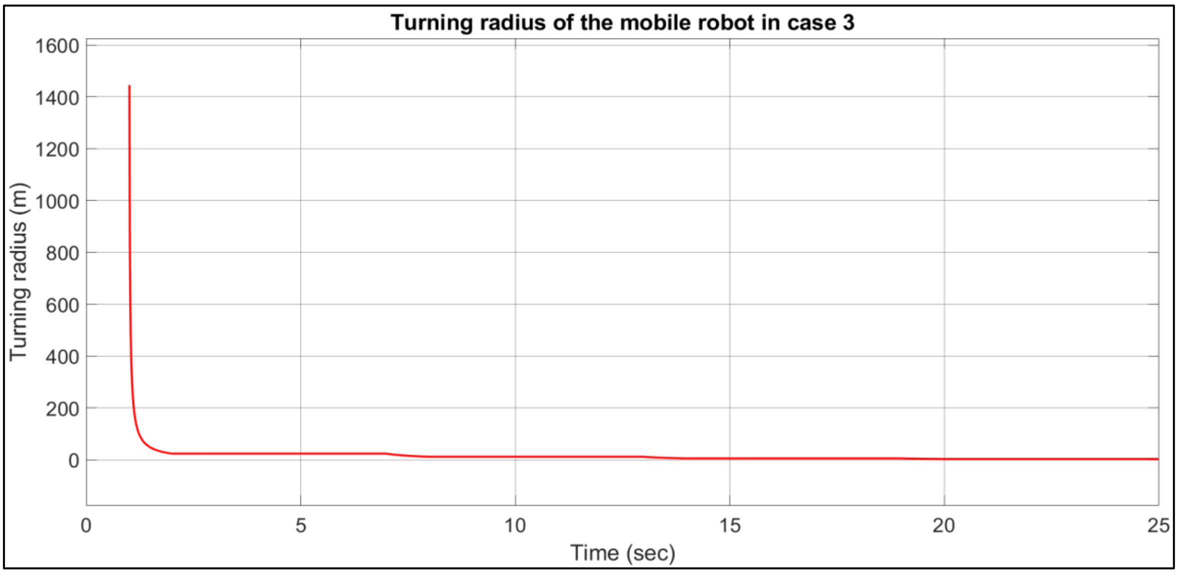

Fig 14 Turning Radius in Method 3

Table 4 Detailed Turning Radius for Method 3

| Steering Angle ($^0$) | Turning Radius (m) |
|---|---|
| -5 | 23,78 |
| -10 | 11,62 |
| -20 | 5,28 |
| -30 | 2,95 |

➢ *Analysis of Experimental Results*

To evaluate the accuracy and reliability of the steering control models, physical laboratory experiments were conducted under the exact scenarios defined in the numerical simulations. To ensure statistical consistency, the experimental trials for each target steering angle were repeated ten times. The averaged empirical data, collected via the optical encoders, alongside the theoretical simulation references, are compiled in Table 5.

Table 5 Experimental Results of the Model Under Different Control Methods

| Method | t (s) | δ ($^0$) | Case | $\delta_{fl}$ ($^0$) | $\delta_{fr}$ ($^0$) | $\delta_{rl}$ ($^0$) | $\delta_{rr}$ ($^0$) |
|---|---|---|---|---|---|---|---|
| Số 1 | 5 | -5 | Sim | -5.16 | -4.85 | 0 | 0 |
| | | | Exp | -5.30 | -4.74 | 0 | 0 |
| | 11 | -10 | Sim | -10.67 | -9.41 | 0 | 0 |
| | | | Exp | -10.76 | -9.40 | 0 | 0 |
| | 17 | -20 | Sim | -22.77 | -17.81 | 0 | 0 |
| | | | Exp | -22.50 | -17.52 | 0 | 0 |
| | 23 | -30 | Sim | -36.19 | -25.49 | 0 | 0 |
| | | | Exp | -36.16 | -25.34 | 0 | 0 |
| Số 2 | 5 | -5 | Sim | -4.66 | -5.40 | 6.13 | 7.10 |
| | | | Exp | -4.78 | -5.60 | 6.22 | 7.32 |
| | 11 | -10 | Sim | -8.72 | -11.72 | 11.49 | 15.37 |
| | | | Exp | -8.58 | -12.02 | 11.94 | 15.80 |
| | 17 | -20 | Sim | -15.49 | -27.93 | 20.63 | 35.76 |
| | | | Exp | -15.12 | -28.38 | 21.00 | 36.46 |
| | 23 | -30 | Sim | -20.91 | -49.76 | 28.58 | 59.31 |
| | | | Exp | -20.36 | -50.62 | 28.92 | 60.44 |
| Số 3 | 5 | -5 | Sim | -4.66 | -5.40 | -6.13 | -7.10 |
| | | | Exp | -4.74 | -5.28 | -6.40 | -7.20 |
| | 11 | -10 | Sim | -8.72 | -11.72 | -11.49 | -15.37 |
| | | | Exp | -8.46 | -11.40 | -12.02 | -15.78 |
| | 17 | -20 | Sim | -15.49 | -27.93 | -20.63 | -35.76 |
| | | | Exp | -14.88 | -27.24 | -21.50 | -36.60 |
| | 23 | -30 | Sim | -20.91 | -49.76 | -28.58 | -59.31 |
| | | | Exp | -20.10 | -48.66 | -29.76 | -60.78 |

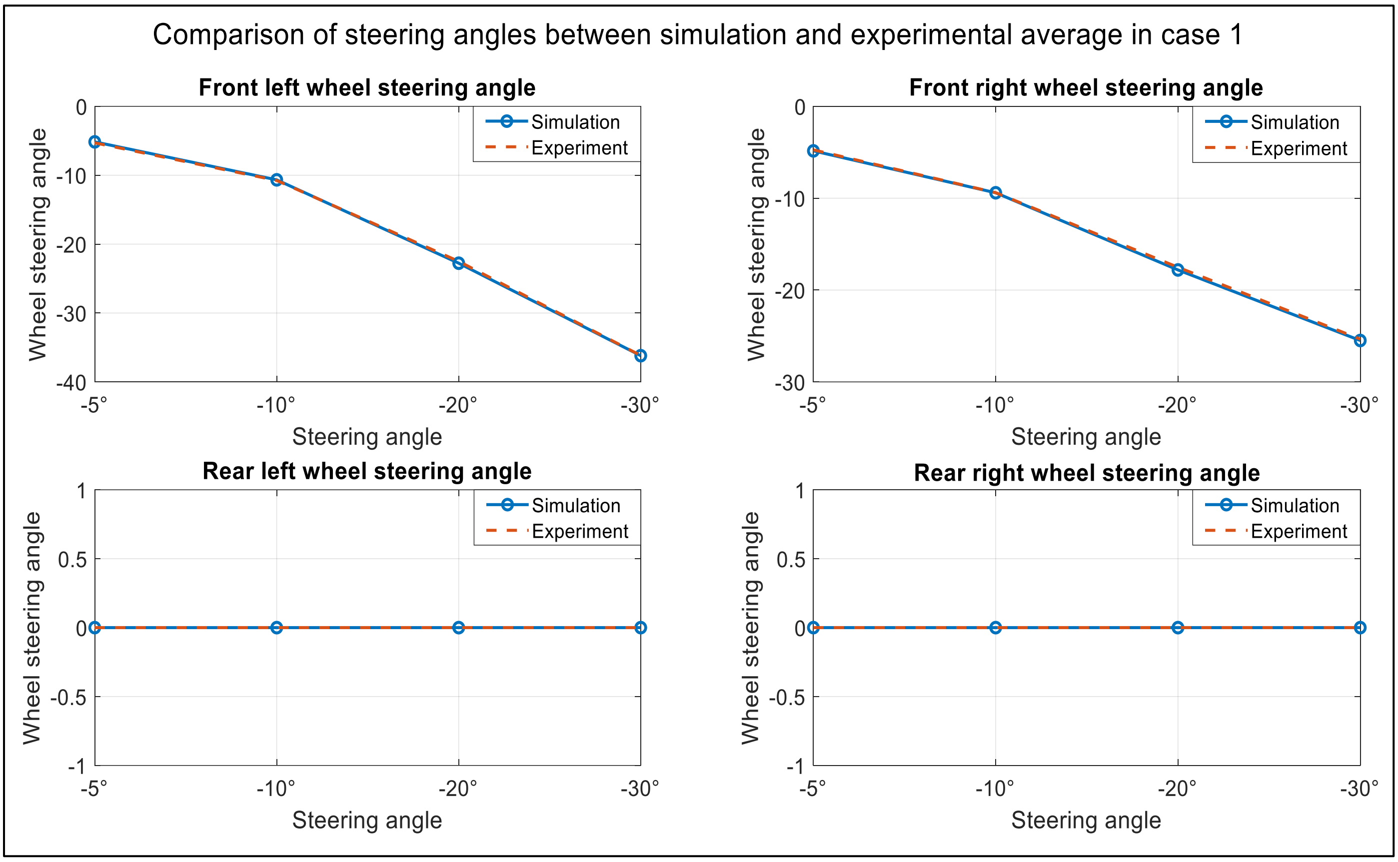


Fig 15 Comparison of Empirical and Simulated Trajectories in Method 1

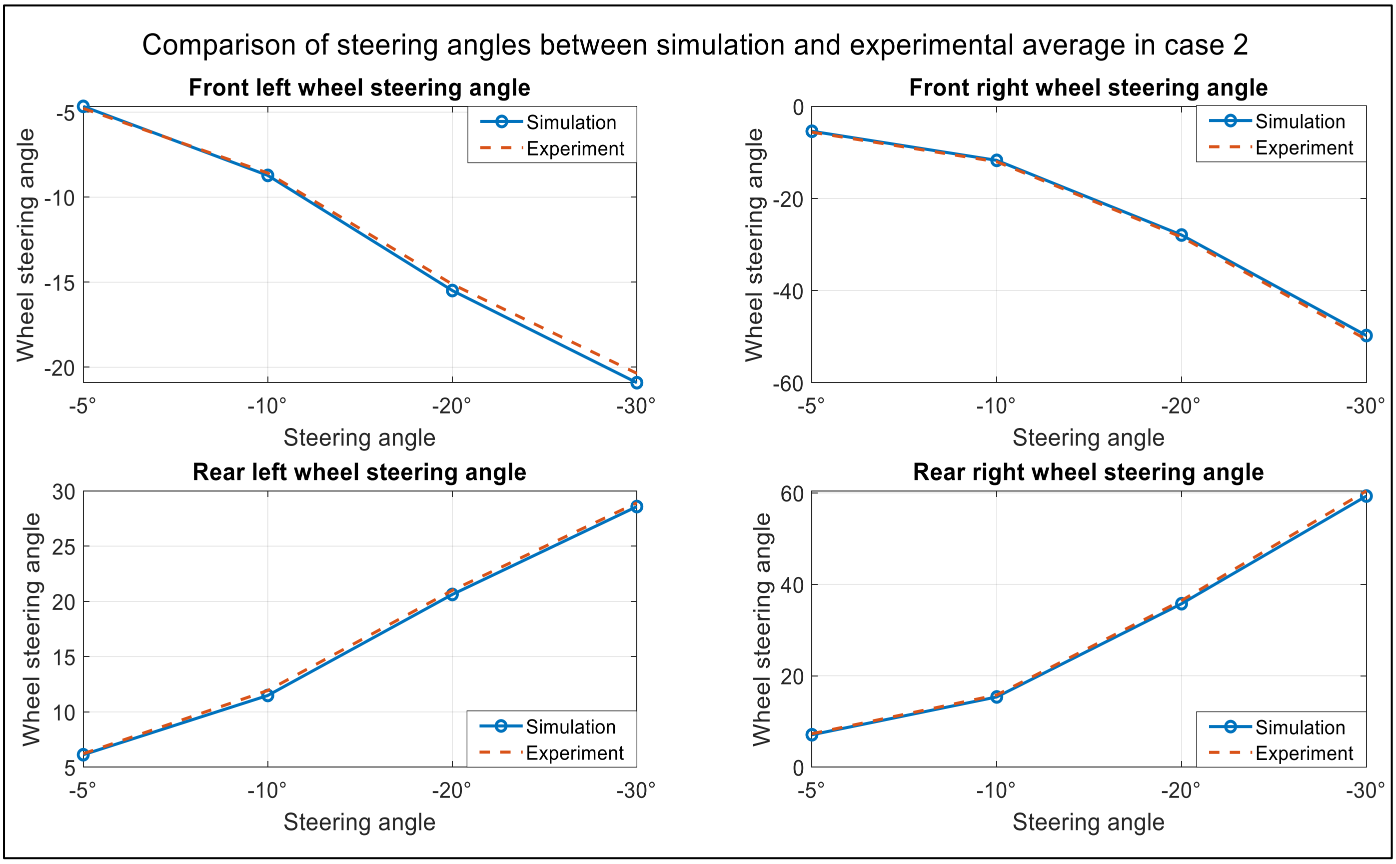


Fig 16 Comparison of Empirical and Simulated Trajectories in Method 2

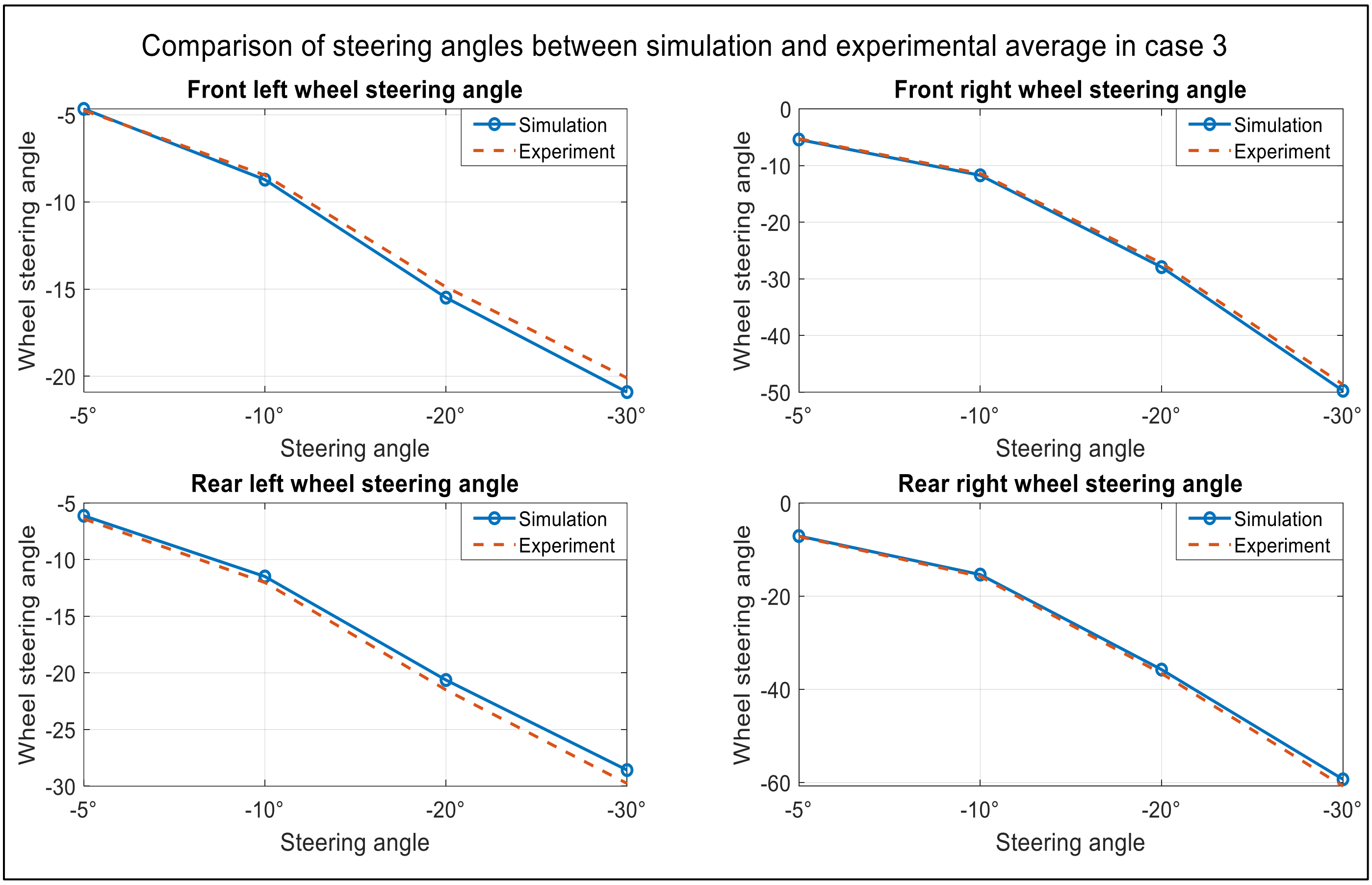


Fig 17 Comparison of Empirical and Simulated Trajectories in Method 3

The continuous time-domain tracking trajectories for the three steering methods are graphically illustrated in Fig. 15, Fig. 16, and Fig. 17. A comparative analysis reveals that the empirical values closely map the simulation trends across all configurations. For Method 1 (two-front-wheel steering), the relative steady-state error is observed to be less than 3% (Fig. 15). This high tracking precision is primarily attributed to the simplicity of the mechanical actuation; since the rear wheels remain fixed, complex multi-axle kinematic conflicts are minimized. In Method 2 (four-wheel opposite-direction steering), the angular tracking error is consistently maintained below 4% (Fig. 16). Although all four wheels are actuated simultaneously, the opposite-phase geometry naturally compels the wheels to follow concentric trajectories around a common instantaneous center of rotation. Consequently, lateral tire scrubbing is significantly reduced, which alleviates the mechanical load on the stepper motors and preserves tracking accuracy.

Conversely, in Method 3 (four-wheel same-direction steering, Fig. 17), a slightly higher relative error is recorded, fluctuating between 1.41% and 3.94% for the front wheels, and 2.35% to 4.61% for the rear wheels. This slight degradation in tracking performance can be explained by the physical constraints of the in-phase steering maneuver. When all wheels are steered in the same direction, the vehicle undergoes a diagonal translation that induces higher lateral friction and structural compliance on the wheel assemblies. Furthermore, minor mechanical backlash within the 1:15 worm gear reducers and unmodeled internal friction become more pronounced under these elevated lateral loads, causing the PID controllers to slightly deviate from the idealized references.

Despite these minor transient and steady-state deviations, the maximum observed error of 4.61% remains well within the acceptable mathematical tolerance for mechatronic kinematics [16]. Therefore, the overall accuracy of the embedded inverse kinematic equations and the hardware robustness of the physical prototype are successfully validated [17]. The empirical framework confirms that the proposed decentralized control algorithms can effectively manage the actuation synchronization required for highly maneuverable autonomous platforms.

## IV. CONCLUSION

Three independent steering control configurations for mobile robots were comprehensively modeled, simulated, and empirically validated in this research. Through the integration of MATLAB/Simulink numerical simulations and physical prototype evaluations, the kinematic performance of two-front-wheel, four-wheel opposite-phase, and four-wheel inphase steering systems was objectively compared. High reliability was demonstrated by the experimental data, which closely matched the theoretical trajectories with a maximum relative error of less than 4%. Based on the comparative analysis, it is concluded that while traditional front-wheel steering benefits from mechanical simplicity, it is highly susceptible to lateral kinematic slip at elevated steering angles. Conversely, the turning radius is significantly minimized by the four-wheel

ISSN No:-2456-2165 https://doi.org/10.38124/ijisrt/26jun1365

opposite-phase steering method, thereby optimizing maneuverability in constrained environments. Furthermore, efficient oblique translational movements are facilitated by the four-wheel in-phase steering configuration without altering the fundamental heading of the platform. Ultimately, a robust theoretical and practical foundation is established by these findings for the design and deployment of highly flexible mobile robotic platforms tailored for complex industrial and agricultural applications.

## ACKNOWLEDGMENT

This research was fully funded by Tra Vinh University under contract number 54/2024/HD.HDKH&DT-DHTV.

## REFERENCES


[1]. R. Nourbakhsh et al., Introduction to Autonomous Mobile Robots, 2nd ed. MIT Press, 2011.

[2]. R. Siegwart, I. R. Nourbakhsh, and D. Scaramuzza, Autonomous Mobile Robots, 2nded. MIT Press, 2011.

[3]. H. D. Liem, P. Q. Phong, and D. V. Kien, "Design of an independent two-wheel drive system for an electric vehicle," Journal of Science and Development Economics, no. 1, pp. 70–78, 2026, doi: 10.64632/jsde.eng.1.2026.715.

[4]. P. Q. Phong, H. D. Liem, and D. V. Kien, "Design and experiment of independent FourWheel Drive system for electric vehicles," UD-JST, vol. 24, no. 1, pp. 1–6, Feb. 2026, doi: 10.31130/ud-jst.2026.24(1).616E.

[5]. L. Q. Chuan, P. Q. Phong, and T. M. Trong, "Investigation of Steering Angle Influence on the Velocities of Four Independently Driven Wheels for a Mobile Robot," International Journal of Innovative Science and Research Technology, vol. 11, no. 5, pp. 3282–3290, May 2026, doi: 10.38124/ijisrt/26May1953.

[6]. J. Y. Wong, Theory of Ground Vehicles, 4th ed. Wiley, 2008.

[7]. H. Sakai, T. Matsuo, S. Murayama, H. Hoshino, and R. Nagashima, "Geometry of a Four-Wheel-Steered Off-Road Vehicle," Journal of Forest Engineering, vol. 4, no. 1, pp. 7–14, 1992, doi: 10.1080/08435243.1992.10702639.

[8]. H. Zheng, S. Yang, and B. Li, "Optimization Control for 4WIS Electric Vehicle Based on the Coincidence Degree of Wheel Steering Centers," SAE Int. J. Veh. Dyn., Stab, and NVH, vol. 2, no. 3, pp. 169–184, 2018, doi: 10.4271/10-02-03-0011.

[9]. J. S. L. Leong, K. T. K. Teo, and H. P. Yoong, "Four Wheeled Mobile Robots: A Review," in 2022 IEEE International Conference on Artificial Intelligence in Engineering and Technology (IICAIET), Kota Kinabalu, Malaysia, 2022, pp. 1–6, doi: 10.1109/IICAIET55139.2022.9936855.

[10]. H. Yin, W. Yi, J. Wu, K. Wang, and J. Guan, "Adaptive Fuzzy Neural Network PID Algorithm for BLDCM Speed Control System," Mathematics, vol. 10, no. 1, p. 118, 2022, doi: 10.3390/math10010118.

[11]. H. Yin, W. Yi, K. Wang, J. Guan, and J. Wu, "Research on Brushless DC Motor Control System Based on Fuzzy Parameter Adaptive PI Algorithm," AIP Advances, vol. 10, no. 10, p. 105208, 2020, doi: 10.1063/5.0025000.

[12]. R. Rajamani, Vehicle Dynamics and Control, 2nd ed. New York, NY, USA: Springer, 2012.

[13]. P. Hang and X. Chen, "Towards Autonomous Driving: Review and Perspectives on Configuration and Control of Four-Wheel Independent Drive/Steering Electric Vehicles," Actuators, vol. 10, no. 8, p. 184, 2021, doi: 10.3390/act10080184.

[14]. Y. H. Kang, D. C. Pang, and Y. C. Zeng, "Optimal dimensional synthesis of Ackermann steering mechanisms for three-axle, six-wheeled vehicles," Applied Sciences, vol. 15, no. 2, p. 589, 2025, doi: 10.3390/app15020800.

[15]. A. N. Kosmidis et al., "Analysis and simulation of four-wheel independent steering control for electric vehicles," AIP Conference Proceedings, vol. 2307, no. 1, p. 020010, 2020, doi: 10.1063/5.0035180.

[16]. Y. Wu, A. Klimchik, A. Pashkevich, S. Caro, and B. Furet, "Industry-oriented performance measures for design of robot calibration experiment," IEEE Robotics and Automation, 2012, doi: 10.1007/978-94-007-4902-3 55.

[17]. M. Franaszek, G. S. Cheok, and J. A. Marvel, "Comparative Study of Two Pose Measuring Systems Used to Reduce Robot Localization Error," Sensors, vol. 20, no. 5, p. 1305, 2020, doi: 10.3390/s20051305.